AIAA JOURNAL
Vol. 43, No. 6, June 2005

First-Order Shear Deformation, *p*-Version, Finite Element for Laminated Plate Nonlinear Vibrations

Pedro Ribeiro*
Universidade do Porto, 4200-465 Porto, Portugal

A *p*-version, hierarchical finite element for moderately thick composite laminated plates is presented, where the effects of the rotary inertia, transverse shear, and geometrical nonlinearity are taken into account. The time-domain free-vibration equations of motion are obtained by applying the principle of virtual work. Those equations are mapped into the frequency domain by the harmonic balance method and solved by a predictor–corrector procedure. The linear natural frequencies of vibration of several plates are determined, and the convergence properties of the element are investigated. It is shown that the element is not prone to shear locking and that a moderate number of degrees of freedom is sufficient for accuracy. The influences of the plate's thickness, of the width to length ratio, and of the fiber orientation on nonlinear free vibrations are investigated.

I. Introduction

BECAUSE of their high stiffness to weight ratio and good resistance to fatigue, composite laminated plates can be found in high-performance structures, where large dynamic loads are applied and where they can easily undergo large-amplitude, geometrically nonlinear vibrations. In this case, the resonance frequency and the nonlinear mode shape are amplitude dependent.[1−4] Therefore, it is important to define the relations between the amplitude and the natural frequency of vibration, that is, the backbone curves, and between the amplitude and the mode shapes of composite laminated plates.

Finite element models based on thin-plate theory[5,6] have been employed to study nonlinear vibrations of laminated plates (Refs. 1–5 and 7, for example). Thin-plate theory, which assumes that planes normal to the midplane remain straight and normal to the plane after deformation, underpredicts deflections and overpredicts natural frequencies. In the fiber direction, composite laminates are strong and stiff, but in the thickness direction the fibers are not so effective, and the shear properties are dominated by the weaker matrix material. Therefore, composite laminated plates have relatively low transverse shear stiffness, and the thin-plate theory assumption is not valid for thicker plates or for higher-order mode analysis, where the wavelength is small when compared to the plate's thickness.[8−10] In these cases, an improved approximation results from considering that planes normal to the midplane remain straight, but not necessarily normal to it, after deformation. This assumption results in what is usually termed first-order shear deformation theory, which has also been followed by many authors regarding linear and nonlinear dynamics.[7−22] For very thick plates, which in some cases might be better not to define as plates to begin with, or for stress determination near regions of discontinuity, higher-order or three-dimensional theories are advisable.[22]

A short review of publications on laminated plates might begin with Ref. 11, in which geometrically nonlinear random vibrations are studied and the transverse shear effects are included, but in which the rotary inertia effects are neglected. The analysis is restricted to single-mode response, a deflection function that represents the first mode is assumed, and the Galerkin method is applied. It is found that the effects of transverse shear are considerable if the plate length is less than 20 times the thickness. Reddy and Chao carried out several analyses using first- and higher-order shear deformations theories. For example, in Ref. 12, the large deflection bending and large-amplitude free vibrations of laminated composite and isotropic plates are analyzed by the finite element method, following the first-order shear deformation theory. Chen and Liu studied the static deflections and linear natural frequencies of isotropic and laminated composite Mindlin plates using a Levy-type solution (see Ref. 15). Ganapathi et al.[16] used a shear flexible element with five nodal degrees of freedom and eight nodes to investigate large-amplitude free flexural vibrations of laminated orthotropic and isotropic plates. In Ref. 17, the vibration of shear deformable angle-ply plates and panels are investigated using the Ritz method. Only linear vibrations are studied.

First-order transverse shear deformation theory has the advantages that it requires only C^0 continuity, that it includes the transverse shear strain in the formulation, and that it is still relatively simple. A disadvantage is that common first-order shear deformation theory (FSDT) finite elements are subjected to shear locking effects.[13,14,20,21] This may be avoided by reduced and selective integration,[13] but spurious modes or an hourglass can occur instead. Brockman[20] addresses the issue of controlling spurious modes of response in linear vibration.

The solutions of systems of nonlinear finite element equations are obtained by iterative methods, and, thus, the number of degrees of freedom (DOF) should be as small as possible. The *p*-version hierarchical finite element method (HFEM) has been applied to study the free vibration of thin isotropic plates with geometrical nonlinearity.[1−4] Several demonstrative examples and theoretical proofs of the advantages of the *p*-version FEM can be found in the literature.[1−4,6,23,24] Recall that the advantages of the *p* version are not limited to the greater convergence rate. In fact, with *h* methods, the accuracy of the solution is determined by executing several analyses with different meshes, an expensive and time-consuming process, both because of the computational cost and because of the operator time required to define the different models. In *p*-convergent approximations, the number of finite elements is determined by the geometry and is small. Moreover, to verify the results, the order of the approximation can be selectively increased. This operation is carried out very efficiently because it is not necessary to generate a new mesh and because the new linear stiffness and mass matrices contain the preceding ones. The previous nonlinear matrices may also be employed in the construction of the improved ones. Finally, if orthogonal functions are employed in the *p* version, the linear matrices are not merely sparse, they are also diagonal.

In this paper, a *p*-version HFEM for moderately thick, rectangular, composite-laminated plates is derived, and geometrically

Presented as Paper 2003-1711 at the AIAA/ASME/ASCE/AHS 44th Structures, Structural Dynamics, and Materials Conference, Norfolk, VA, 7–10 April 2003; received 22 July 2003; revision received 12 November 2004; accepted for publication 22 December 2004.

*Assistant Professor, Department of Mechanical Engineering, Instituto de Engenharia Mecânica, Faculdade de Engenharia, Rua Dr. Roberto Frias s/n; pmleal@fe.up.pt. Member AIAA.

nonlinear free vibrations with amplitudes of the order of the plates' thicknesses are studied. Unlike in Refs. 2–4, where thin-plate theory was followed, the transverse shear strains and the rotary inertia are also considered in this work. The in-plane displacements' effects are considered as well. The harmonic balance method is applied to derive the equations of motion in the frequency domain, which are solved by a continuation method. The convergence properties of the element and the influence of the plate's thickness on the backbone curves and on the nonlinear mode shapes of plates with different width to length ratios are investigated. The first- and higher-order modes are analyzed, and results are compared with published results. Thick to very thin plates are investigated, the latter to show that the element proposed is not prone to shear locking.

II. Plate Element and Equations of Motion

The element derived in this section can be used to study elastic plates with uniform thickness h, width a, and length b. Reissner[8]–Mindlin's[9] formulation, also known as FSDT is followed; thus, the transverse shear deformation and the rotary inertia are considered. The displacement components along the x and y directions, u and v at any point of the plate, are functions of the midplane translations u^0 and v^0 and of the independent rotations of the normal to the midplane about x and y, which are denoted θ_x^0 and θ_y^0 (Fig. 1). The superscript zero represents the midplane. The displacement along the z direction, w, depends only on x and y. Hence, the displacement components of a particle with coordinates (x, y, z) are

$$u(x, y, z, t) = u^0(x, y, t) + z\theta_y^0(x, y, t) \tag{1}$$

$$v(x, y, z, t) = v^0(x, y, t) - z\theta_x^0(x, y, t) \tag{2}$$

$$w(x, y, z, t) = w^0(x, y, t) \tag{3}$$

The strain-displacement relationships are

$$\varepsilon_x = \varepsilon_x^0 - z\kappa_x \tag{4}$$

$$\varepsilon_y = \varepsilon_y^0 - z\kappa_y \tag{5}$$

$$\gamma_{xy} = \gamma_{xy}^0 - z\kappa_{xy} \tag{6}$$

$$\gamma_{zx} = \gamma_{zx}^0 \tag{7}$$

$$\gamma_{yz} = \gamma_{yz}^0 \tag{8}$$

where ε_x^0, ε_y^0, and γ_{xy}^0 are the in-plane strain components at $z = 0$, defined by the following nonlinear strain-displacement relationships[6]:

$$\varepsilon_x^0 = u_{,x}^0 + \tfrac{1}{2}\left(w_{,x}^0\right)^2, \qquad \varepsilon_y^0 = v_{,y}^0 + \tfrac{1}{2}\left(w_{,y}^0\right)^2$$
$$\gamma_{xy}^0 = u_{,y}^0 + v_{,x}^0 + w_{,x}^0 w_{,y}^0 \tag{9}$$

where, for instance, $u_{,x}^0$ represents the partial derivative $\partial u^0/\partial x$. The terms κ_x, κ_y, and κ_{xy} in Eqs. (4–6) are the plate curvatures, which are given by

$$\kappa_x = -\frac{\partial \theta_y^0}{\partial x}, \qquad \kappa_y = \frac{\partial \theta_x^0}{\partial y}, \qquad \kappa_{xy} = -\frac{\partial \theta_y^0}{\partial y} + \frac{\partial \theta_x^0}{\partial x} \tag{10}$$

The transverse shear strains are

$$\gamma_{zx}^0 = w_{,x}^0 + \theta_y^0, \qquad \gamma_{yz}^0 = w_{,y}^0 - \theta_x^0 \tag{11}$$

For each element, the middle plane displacements and the rotations are expressed in the form

$$\begin{Bmatrix} u^0 \\ v^0 \\ w^0 \\ \theta_y^0 \\ \theta_x^0 \end{Bmatrix} = \begin{bmatrix} \{N^u\}^T & 0 & 0 & 0 & 0 \\ 0 & \{N^u\}^T & 0 & 0 & 0 \\ 0 & 0 & \{N^w\}^T & 0 & 0 \\ 0 & 0 & 0 & \{N^{\theta_y}\}^T & 0 \\ 0 & 0 & 0 & 0 & \{N^{\theta_x}\}^T \end{bmatrix} \begin{Bmatrix} q_u \\ q_v \\ q_w \\ q_{\theta_y} \\ q_{\theta_x} \end{Bmatrix} \tag{12}$$

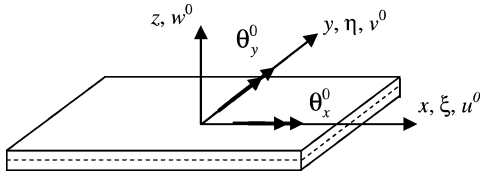

Fig. 1 Plate element.

where $\{q_u\}$, $\{q_v\}$, and $\{q_w\}$ are the vectors of generalized in- and out-of-plane displacements and $\{q_{\theta_y}\}$ and $\{q_{\theta_x}\}$ are the vectors of generalized rotations. The complete matrix of shape functions $[N]$ is constituted by the row vectors of bidimensional in-plane, out-of-plane, and rotational shape functions, which are, respectively,

$$\{N^u\}^T = \{g_1(\xi)g_1(\eta), g_1(\xi)g_2(\eta), \ldots, g_{p_i}(\xi)g_{p_i}(\eta)\} \tag{13}$$

$$\{N^w\}^T = \{f_1(\xi)f_1(\eta), f_1(\xi)f_2(\eta), \ldots, f_{p_o}(\xi)f_{p_o}(\eta)\} \tag{14}$$

$$\{N^{\theta_y}\}^T = \left\{\theta_{y_1}(\xi)\theta_{y_1}(\eta), \theta_{y_1}(\xi)\theta_{y_2}(\eta), \ldots, \theta_{y_{p_{\theta y}}}(\xi)\theta_{y_{p_{\theta y}}}(\eta)\right\} \tag{15}$$

$$\{N^{\theta_x}\}^T = \left\{\theta_{x_1}(\xi)\theta_{x_1}(\eta), \theta_{x_1}(\xi)\theta_{x_2}(\eta), \ldots, \theta_{x_{p_{\theta x}}}(\xi)\theta_{x_{p_{\theta x}}}(\eta)\right\} \tag{16}$$

The vectors $\{g\}$, $\{f\}$, $\{\theta_y\}$, and $\{\theta_x\}$ are the vectors of in-plane, transverse, and rotational one-dimensional displacement shape functions; p_o, p_i, p_{θ_y}, and p_{θ_x} are the numbers of transverse, middle plane, rotation about y, and rotation about x displacement shape functions employed; and ξ and η are the local coordinates.

One is free to choose the number and set of displacement shape functions to be applied in the definition of the element. With regard to the transverse displacements, Legendre polynomials in Rodrigues's form, plus the four Hermite cubics, have been used extensively (see Refs. 1–4 and 25). They require a small number of DOF, and the boundary conditions are easily implemented because only one of the first Hermite cubics has either displacement or rotation different from zero at the end of each element. All of the Legendre polynomials in Rodrigues's form have zero amplitudes and slopes at $\xi = -1$ and $\xi = 1$. This set of functions will be used here. A set of polynomials called the g set[1–4] will be applied in conjunction with linear functions for the in-plane displacement, as well as for the rotation fields. Their value is zero at the boundaries, but their derivatives are not zero.

Continuous plate structures are analyzed in this work. In similar cases, it has been demonstrated that, for the same number of DOF, the solution arising from a single element is more accurate than that calculated with more elements.[25] With the origin of the coordinate axes located at the center of the plate, the local and global coordinates are related by

$$\xi = 2x/a, \qquad \eta = 2y/b \tag{17}$$

and, consequently, the matrices derived in the following paragraphs are simultaneously element and complete system matrices. When more than one element is employed, the assembly of the element matrices is carried out in the usual way.[6,10]

Using the plane stress constitutive equation for the kth layer,[26] we have

$$\begin{Bmatrix} \sigma_x^{(k)} \\ \sigma_y^{(k)} \\ \tau_{yz}^{(k)} \\ \tau_{xz}^{(k)} \\ \tau_{xy}^{(k)} \end{Bmatrix} = \begin{bmatrix} C_{11}^{(k)} & C_{12}^{(k)} & 0 & 0 & C_{16}^{(k)} \\ C_{12}^{(k)} & C_{22}^{(k)} & 0 & 0 & C_{26}^{(k)} \\ 0 & 0 & C_{44}^{(k)} & C_{45}^{(k)} & 0 \\ 0 & 0 & C_{54}^{(k)} & C_{55}^{(k)} & 0 \\ C_{16}^{(k)} & C_{26}^{(k)} & 0 & 0 & C_{66}^{(k)} \end{bmatrix} \begin{Bmatrix} \varepsilon_x^{(k)} \\ \varepsilon_y^{(k)} \\ \gamma_{yz}^{(k)} \\ \gamma_{xz}^{(k)} \\ \gamma_{xy}^{(k)} \end{Bmatrix} \tag{18}$$

where $C_{ij}^{(k)}$ are the reduced stiffnesses of the kth layer, which can be obtained from the E_1 and E_2 major and minor Young's moduli, from the Poisson's ratios ν_{12} and ν_{21}, and from the shear moduli G_{12},

G_{13}, and G_{23} (Ref. 22). The subscripts 1 and 2 denote the principal directions of the orthotropic plate layer. A shear correction factor that accounts for the fact that the shear stresses are not constant across the section[6,8] is employed. Although the value proposed by Reissner,[8] $\lambda = \frac{5}{6}$, is used herein, Noor and Burton[27] suggest that, for greater accuracy, the values of the shear correction factor should depend on the lamination and on the geometric parameters of the plate.

The in-plane strain components are given by

$$\begin{Bmatrix} \varepsilon_x \\ \varepsilon_y \\ \gamma_{xy} \end{Bmatrix} = \begin{bmatrix} 1 & 0 & 0 & -z & 0 & 0 \\ 0 & 1 & 0 & 0 & -z & 0 \\ 0 & 0 & 1 & 0 & 0 & -z \end{bmatrix} \{\varepsilon\} = [[I] - z[I]]\{\varepsilon\} \tag{19}$$

with

$$\{\varepsilon\} = \begin{Bmatrix} \varepsilon_o^p \\ \varepsilon_o^b \end{Bmatrix} + \begin{Bmatrix} \varepsilon_L^p \\ 0 \end{Bmatrix} \tag{20}$$

The linear in-plane and bending strains $\{\varepsilon_o^p\}$ and $\{\varepsilon_o^b\}$ and the geometrically nonlinear in-plane strain $\{\varepsilon_L^P\}$ are defined as

$$\left\{\varepsilon_o^p\right\} = \begin{Bmatrix} u^0_{,x} \\ v^0_{,y} \\ u^0_{,y} + v^0_{,x} \end{Bmatrix}, \qquad \left\{\varepsilon_o^b\right\} = \begin{Bmatrix} -\dfrac{\partial \theta_y^0}{\partial x} \\ \dfrac{\partial \theta_x^0}{\partial y} \\ -\dfrac{\partial \theta_y^0}{\partial y} + \dfrac{\partial \theta_x^0}{\partial x} \end{Bmatrix}$$

$$\left\{\varepsilon_L^p\right\} = \begin{Bmatrix} \dfrac{\left(w^0_{,x}\right)^2}{2} \\ \dfrac{\left(w^0_{,y}\right)^2}{2} \\ w^0_{,x} w^0_{,y} \end{Bmatrix} \tag{21}$$

The transverse shear strains are

$$\begin{Bmatrix} \gamma_{zx} \\ \gamma_{yz} \end{Bmatrix} = \begin{Bmatrix} w^0_{,x} + \theta_y \\ w^0_{,y} - \theta_x \end{Bmatrix} \tag{22}$$

For the sake of completeness, the strain-displacement relations are given as functions of the element shape functions and generalized displacements in the Appendix.

The in-plane stress resultants and the moments, all per unit length, are, respectively, defined by

$$\{T_x, T_y, T_{xy}\} = \int_{-h/2}^{h/2} \{\sigma_x, \sigma_y, \tau_{xy}\}\, \mathrm{d}z \tag{23}$$

$$\{M_x, M_y, M_{xy}\} = \int_{-h/2}^{h/2} \{\sigma_x, \sigma_y, \tau_{xy}\} z\, \mathrm{d}z \tag{24}$$

The shear stress resultants in the x and y directions, are, respectively, the following:

$$\{Q_x, Q_y\} = \int_{-h/2}^{h/2} \{\tau_{xz}, \tau_{yz}\}\, \mathrm{d}z \tag{25}$$

Substituting Equation (18) into Eqs. (23–25), one arrives at the constitutive relations of the plate:

$$\begin{Bmatrix} T \\ M \end{Bmatrix} = \begin{bmatrix} [A] & [B] \\ [B] & [D] \end{bmatrix} \left(\begin{Bmatrix} \varepsilon_o^p \\ \varepsilon_o^b \end{Bmatrix} + \begin{Bmatrix} \varepsilon_L^p \\ 0 \end{Bmatrix} \right) \tag{26}$$

$$\begin{Bmatrix} Q_x \\ Q_y \end{Bmatrix} = \begin{bmatrix} C_{55} & C_{54} \\ C_{45} & C_{44} \end{bmatrix} \begin{Bmatrix} \gamma_{zx} \\ \gamma_{yz} \end{Bmatrix} \tag{27}$$

The membrane, coupling, and flexural rigidity are symmetric matrices given by

$$(A_{ij}, B_{ij}, D_{ij}) = \sum_{k=1}^{NL} \int_{z_{k-1}}^{z_k} (1,\ z,\ z^2) C_{ij}^{(k)}\, \mathrm{d}z, \qquad i, j = 1, 2, \text{and } 6$$

$$C_{ij} = \sum_{k=1}^{NL} \int_{z_{k-1}}^{z_k} C_{ij}^{(k)}\, \mathrm{d}z, \qquad i, j = 4, 5$$

Because only symmetric laminated plates will be analyzed, there is no coupling between in-plane stretching and transverse bending; therefore, $B_{ij} = 0$.

The plate equations of motion are derived by equating the sum of the virtual work of the inertia forces and of the elastic restoring forces to zero. The virtual work of the internal forces is

$$\delta W_{in} = -\int_\Omega \{\delta\varepsilon\}^T \begin{Bmatrix} T \\ M \end{Bmatrix} \mathrm{d}\Omega - \int_\Omega \{\delta\gamma\}^T \{Q\}\, \mathrm{d}\Omega \tag{28}$$

or, as function of the deformations,

$$\delta W_{in} = -\int_\Omega \left(\begin{Bmatrix} \delta\varepsilon_o^p \\ \delta\varepsilon_o^b \end{Bmatrix}^T + \begin{Bmatrix} \delta\varepsilon_L^p \\ 0 \end{Bmatrix}^T \right) \begin{bmatrix} [A] & [0] \\ [0] & [D] \end{bmatrix} \times \left(\begin{Bmatrix} \varepsilon_o^p \\ \varepsilon_o^b \end{Bmatrix} + \begin{Bmatrix} \varepsilon_L^p \\ 0 \end{Bmatrix} \right) \mathrm{d}\Omega - \int_\Omega \{\delta\gamma\}^T [C] \{\gamma\}\, \mathrm{d}\Omega \tag{29}$$

From Eq. (29), the in-plane linear stiffness matrix $[K_{1_p}]$, which is equal to the thin-plate matrix given in Ref. 4, as well as the bending and shear linear stiffness matrices result. The latter are given by

$$[K_{1b}] = \int_\Omega \begin{bmatrix} -\left\{N_{,x}^{\theta_y}\right\} & 0 & -\left\{N_{,y}^{\theta_y}\right\} \\ 0 & \left\{N_{,y}^{\theta_x}\right\} & \left\{N_{,x}^{\theta_x}\right\} \end{bmatrix} \begin{bmatrix} D_{11} & D_{12} & D_{13} \\ D_{12} & D_{22} & D_{23} \\ D_{13} & D_{23} & D_{66} \end{bmatrix} \times \begin{bmatrix} -\left\{N_{,x}^{\theta_y}\right\}^T & 0 \\ 0 & \left\{N_{,y}^{\theta_x}\right\}^T \\ -\left\{N_{,y}^{\theta_y}\right\}^T & \left\{N_{,x}^{\theta_x}\right\}^T \end{bmatrix} \mathrm{d}\Omega \tag{30}$$

$$\left[K_1^\gamma\right] = \lambda \int_\Omega \begin{bmatrix} \left\{N_{,x}^w\right\} & \left\{N_{,y}^w\right\} \\ \{N^{\theta_y}\} & 0 \\ 0 & -\{N^{\theta_x}\} \end{bmatrix} \begin{bmatrix} C_{55} & C_{54} \\ C_{45} & C_{44} \end{bmatrix} \times \begin{bmatrix} \left\{N_{,x}^w\right\}^T & \{N^{\theta_y}\}^T & 0 \\ \left\{N_{,y}^w\right\}^T & 0 & -\{N^{\theta_x}\}^T \end{bmatrix} \mathrm{d}\Omega \tag{31}$$

The nonlinear stiffness matrices $[K_2\{q_w\}]$ and $[K_4\{q_w\}]$ also result from Eq. (29). Matrix $[K_2\{q_w\}]$ depends linearly on the generalized transverse displacements $\{q_w\}$, and matrix $[K_4\{q_w\}]$ depends quadratically. These matrices are equal to the thin-plate theory matrices, again given in Ref. 4. Matrix $[K_3]$ is equal to $2[K_2]^T$ (Ref. 1).

The virtual work of the inertia forces is

$$\delta W_j = -\int_{-h/2}^{h/2} \int_\Omega \rho(\delta u \ddot{u} + \delta v \ddot{v} + \delta w \ddot{w})\, \mathrm{d}\Omega\, \mathrm{d}z \tag{32}$$

which is equivalent to

$$\delta W_j = \{\delta q\}^T \left(-\rho h b \int_L [N]^T [N]\, \mathrm{d}L \{\ddot{q}\} \right)$$

$$\Leftrightarrow \delta W_j = \{\delta q\}^T [M] \{\ddot{q}\} \tag{33}$$

where $[M]$ is the mass matrix, which is more explicitly defined as

$$\begin{bmatrix} [M_p] & 0 & 0 & 0 & 0 \\ 0 & [M_p] & 0 & 0 & 0 \\ 0 & 0 & [M_b] & 0 & 0 \\ 0 & 0 & 0 & [M_{Ry}] & 0 \\ 0 & 0 & 0 & 0 & [M_{Rx}] \end{bmatrix}$$

$$= \rho h \begin{bmatrix} \int_\Omega \{N^u\}\{N^u\}^T \mathrm{d}\Omega & 0 & 0 & 0 & 0 \\ 0 & \int_\Omega \{N^u\}\{N^u\}^T \mathrm{d}\Omega & 0 & 0 & 0 \\ 0 & 0 & \int_\Omega \{N^w\}\{N^w\}^T \mathrm{d}\Omega & 0 & 0 \\ 0 & 0 & 0 & \frac{h^2}{12}\int_\Omega \{N^{\theta_y}\}\{N^{\theta_y}\}^T \mathrm{d}\Omega & 0 \\ 0 & 0 & 0 & 0 & \frac{h^2}{12}\int_\Omega \{N^{\theta_x}\}\{N^{\theta_x}\}^T \mathrm{d}\Omega \end{bmatrix} \tag{34}$$

$[M_p]$ and $[M_b]$ are the in-plane and out-of-plane inertia matrices, and $[M_{Ry}]$ and $[M_{Rx}]$ are due to the rotary inertia.

Hence, the free-vibration, time-domain equations of motion in generalized coordinates are

$$\begin{bmatrix} [M_p] & 0 & 0 & 0 & 0 \\ 0 & [M_p] & 0 & 0 & 0 \\ 0 & 0 & [M_b] & 0 & 0 \\ 0 & 0 & 0 & [M_{Ry}] & 0 \\ 0 & 0 & 0 & 0 & [M_{Rx}] \end{bmatrix} \begin{Bmatrix} \ddot{q}_u \\ \ddot{q}_v \\ \ddot{q}_w \\ \ddot{q}_{\theta_y} \\ \ddot{q}_{\theta_x} \end{Bmatrix} + \begin{bmatrix} \left[K_1^{p^{11}}\right] & \left[K_1^{p^{12}}\right] & 0 & 0 & 0 \\ \left[K_1^{p^{12}}\right] & \left[K_1^{p^{22}}\right] & 0 & 0 & 0 \\ 0 & 0 & \left[K_1^{\gamma^{11}}\right] & \left[K_1^{\gamma^{12}}\right] & \left[K_1^{\gamma^{13}}\right] \\ 0 & 0 & \left[K_1^{\gamma^{12}}\right] & \left[K_1^{b^{11}}\right]+\left[K_1^{\gamma^{22}}\right] & \left[K_1^{b^{12}}\right]+\left[K_1^{\gamma^{23}}\right] \\ 0 & 0 & \left[K_1^{\gamma^{13}}\right] & \left[K_1^{b^{12}}\right]+\left[K_1^{\gamma^{23}}\right] & \left[K_1^{b^{22}}\right]+\left[K_1^{\gamma^{33}}\right] \end{bmatrix}$$

$$\times \begin{Bmatrix} q_u \\ q_v \\ q_w \\ q_{\theta_y} \\ q_{\theta_x} \end{Bmatrix} + \begin{bmatrix} 0 & 0 & \left[K_2^{11}\right] & 0 & 0 \\ 0 & 0 & \left[K_2^{21}\right] & 0 & 0 \\ \left[K_3^{11}\right] & \left[K_3^{12}\right] & [K_4] & 0 & 0 \\ 0 & 0 & 0 & 0 & 0 \\ 0 & 0 & 0 & 0 & 0 \end{bmatrix} \begin{Bmatrix} q_u \\ q_v \\ q_w \\ q_{\theta_y} \\ q_{\theta_x} \end{Bmatrix} = \begin{Bmatrix} 0 \\ 0 \\ 0 \\ 0 \\ 0 \end{Bmatrix} \tag{35}$$

The matrices in Eq. (35) were divided into submatrices, as indicated by the superscripts.

Provided that the middle-plane in-plane displacements are much smaller than the transverse displacement, it is a reasonable approximation to neglect the middle-plane inertia, which allows one to condense the equations of motion. In this case, the in-plane generalized displacements are given by

$$\begin{Bmatrix} q_u \\ q_v \end{Bmatrix} = -\begin{bmatrix} \left[K_1^{p^{11}}\right] & \left[K_1^{p^{12}}\right] \\ \left[K_1^{p^{21}}\right] & \left[K_1^{p^{22}}\right] \end{bmatrix}^{-1} \begin{bmatrix} \left[K_2^{11}\right] \\ \left[K_2^{21}\right] \end{bmatrix} \{q_w\} \tag{36}$$

In simplified notation, where, for example,

$$\left[K_1^p\right] = \begin{bmatrix} \left[K_1^{p^{11}}\right] & \left[K_1^{p^{12}}\right] \\ \left[K_1^{p^{21}}\right] & \left[K_1^{p^{22}}\right] \end{bmatrix}$$

and dropping all superscripts, the reduced equations of motion are given by

$$\begin{bmatrix} [M_b] & 0 & 0 \\ 0 & [M_{Ry}] & 0 \\ 0 & 0 & [M_{Rx}] \end{bmatrix} \begin{Bmatrix} \ddot{q}_w \\ \ddot{q}_{\theta_y} \\ \ddot{q}_{\theta_x} \end{Bmatrix}$$

$$+ \begin{bmatrix} \left[K_1^{\gamma}\right] & \left[K_1^{\gamma}\right] & \left[K_1^{\gamma}\right] \\ \left[K_1^{\gamma}\right] & \left[K_1^{b}\right]+\left[K_1^{\gamma}\right] & \left[K_1^{b}\right]+\left[K_1^{\gamma}\right] \\ \left[K_1^{\gamma}\right] & \left[K_1^{b}\right]+\left[K_1^{\gamma}\right] & \left[K_1^{b}\right]+\left[K_1^{\gamma}\right] \end{bmatrix} \begin{Bmatrix} q_w \\ q_{\theta_y} \\ q_{\theta_x} \end{Bmatrix}$$

$$+ \begin{bmatrix} [K_4]-[K_3]\left[K_1^p\right]^{-1}[K_2] & 0 & 0 \\ 0 & 0 & 0 \\ 0 & 0 & 0 \end{bmatrix} \begin{Bmatrix} q_w \\ q_{\theta_y} \\ q_{\theta_x} \end{Bmatrix} = \begin{Bmatrix} 0 \\ 0 \\ 0 \end{Bmatrix} \tag{37}$$

Although nonlinear systems undergo nonharmonic motions, it is reasonable to assume harmonic motion in many cases, particularly for moderate vibration amplitudes. This simplification allows one to obtain a compact frequency-domain model,which provides very

useful information. Thus, harmonic motion will be assumed, and we have

$$\begin{Bmatrix} q_w \\ q_{\theta_y} \\ q_{\theta_x} \end{Bmatrix} = \begin{Bmatrix} Q_w \\ Q_{\theta_y} \\ Q_{\theta_x} \end{Bmatrix} \cos(\omega t) \tag{38}$$

where $\{Q\} = \{\{Q_w\}, \{Q_{\theta_y}\}, \{Q_{\theta_x}\}\}$ is the vector of generalized amplitudes of the harmonic motions. Insertion of Eq. (38) into Eq. (37) and application of the harmonic balance method results in the following frequency-domain equations of motion:

$$\left(-\omega^2 \begin{bmatrix} [M_b] & 0 & 0 \\ 0 & [M_{Ry}] & 0 \\ 0 & 0 & [M_{Rx}] \end{bmatrix} + \begin{bmatrix} [K_1^\gamma] & [K_1^\gamma] & [K_1^\gamma] \\ [K_1^\gamma] & [K_1^b]+[K_1^\gamma] & [K_1^b]+[K_1^\gamma] \\ [K_1^\gamma] & [K_1^b]+[K_1^\gamma] & [K_1^b]+[K_1^\gamma] \end{bmatrix} \right) \begin{Bmatrix} Q_w \\ Q_{\theta_y} \\ Q_{\theta_x} \end{Bmatrix} + \begin{Bmatrix} Fnl \\ 0 \\ 0 \end{Bmatrix} = \begin{Bmatrix} 0 \\ 0 \\ 0 \end{Bmatrix} \tag{39}$$

where the vector $\{Fnl\}$ is a cubic function of the generalized amplitudes $\{Q_w\}$, defined as

$$\{Fnl\} = \frac{2}{T} \int_0^T [Knl(\{Q_w\})]\{Q_w\} \cos(\omega t)\, dt$$

$$\Leftrightarrow \{Fnl\} = \frac{3}{4}\Big([K_4(\{Q_w\})] - 2\big[[K_2(\{Q_w\})]^T \big[K_1^P\big]^{-1} \times [K_2(\{Q_w\})]\big]\Big)\{Q_w\} \tag{40}$$

A symbolic computation package is used to manipulate the shape functions and create the element mass and stiffness matrices. The equations of motion are solved by a continuation method, the details of which can be found in Refs. 3 and 4.

III. Numerical Results

A. Linear Analysis

To validate the element derived and demonstrate its usefulness, a convergence study is carried out, and results are compared with published data. The linear natural frequencies of plates with free edges (FFFF) and of fully clamped plates with immovable edges (CCCC) are investigated. These boundary conditions are easily assigned to the plate by an adequate choice of the shape functions. In the first case, FFFF, the cubic out-of-plane shape functions, the linear in-plane functions, and the linear rotational shape functions, which correspond to edge displacements or rotations different from zero, are used. In the second case, CCCC, none of these functions is included in the element. The same number of rotational shape functions was employed to approximate both rotations, therefore, $p_{\theta_x} = p_{\theta_y} = p_\theta$.

Completely free boundary conditions are of importance due to their practical applications and because they are easily implemented in the laboratory. Thus, we start by comparing the linear natural frequency parameters $\omega(L^2/h)(\rho/E_2)^{1/2}$ of an FFFF rectangular plate with the those of other authors in Table 1. The rectangular plate in question is an angle-ply $[(-45 \text{ deg } /+45 \text{ deg})_8]_{\text{symmetric}}$ plate, with the following dimensions: $a = 0.2$ m, $b = 0.1$ m, and $h = 0.001$ m. Its mass density is $\rho = 1600$ kg/m^3. The major and minor Young's moduli are $E_{11} = 131.7 \times 10^9$ N/m^2 and $E_{22} = 9.86 \times 10^9$ N/m^2, the shear modulus G_{12} is 4.21×10^9 N/m^2, and the Poisson ratio is $\nu_{12} = 0.28$. It will be assumed that G_{13} and G_{23} are equal to G_{12}, but they will be multiplied by the shear correction coefficients $\lambda = \frac{5}{6}$.

In the HFEM, the convergence of the linear natural frequency values always occurs from above. Thus, although theories of different order are compared, it is apparent from the values shown in Table 1 that with 147 DOF the p-version HFEM already gives more accurate values than those in Refs. 21 and 28 for the first two linear natural frequencies. With 386 DOF, lower bound values are computed for at least the first eight natural frequencies.

First-order transverse shear deformation theory has the advantages of requiring only C^0 continuity and of allowing one to study thick plates. However, common finite elements based on FSDT are subject to shear locking,[13,21] implying, amongst other effects, that the natural frequencies of thin plates are overpredicted. To verify how the proposed element deals with shear locking, fully clamped plates with different thicknesses are investigated. All of these CCCC plates have eight layers, the fibers are oriented as $(2\theta, -\theta, \theta, 0)_{\text{sym}}$, and the assumed geometric and material properties are the following: $a = 0.480$ m, $\rho = 1540$ kg/m^3, $E_{11} = 120.5 \times 10^9$ N/m^2, $E_{22} = 9.63 \times 10^9$ N/m^2, $G_{12} = 3.58 \times 10^9$ N/m^2, $G_{13} = 3.58 \times 10^9$ N/m^2, $G_{23} = 3.58 \times 10^9$ N/m^2, and $\nu_{12} = 0.32$. The width b and the angle θ are defined subsequently. Each plate of this type will be called plate 2. First, different thicknesses are assumed: b is 0.320 m and θ is equal to 45 deg.

The first three natural frequencies of plate 2 when $b/h = 320$ are shown in Table 2. Frequencies from Ref. 3, where the thin-plate

Table 1 Linear frequency parameters of FFFF rectangular plate

Mode	Thin-plate theory, Rayleigh–Ritz[a]	Higher-order theory, FEM[21]	HFEM, p version			
			$p_o = 7,\ p_\theta = 7,\ n = 147$	$p_o = 8,\ p_\theta = 8,\ n = 192$	$p_o = 12,\ p_\theta = 11,\ n = 386$	$p_o = 13,\ p_\theta = 13,\ n = 507$
1	8.58	8.60	8.5764	8.576	8.5705	8.5690
2	23.38	23.38	23.315	23.264	23.224	23.197
3	29.19	29.44	29.749	29.081	28.975	28.946
4	45.79	46.10	45.952	45.945	45.635	45.612
5	48.68	48.80	48.532	48.458	48.334	48.267
6	66.74	67.57	69.281	67.700	66.258	66.202
7	68.02	68.14	70.614	70.119	67.281	67.218
8	78.81	——	82.049	78.765	78.093	77.978

[a]See Ref. 28.

Table 2 Linear frequencies of CCCC rectangular plate (radians per second) calculated by p-version HFEM

Mode	Thin-plate theory[3]		First-order shear deformation					
	$p_o = 4,\ n = 16$	$p_o = 7,\ n = 49$	$p_o = 4,\ p_\theta = 6,\ n = 88$	$p_o = 5,\ p_\theta = 7,\ n = 123$	$p_o = 7,\ p_\theta = 7,\ n = 147$	$p_o = 7,\ p_\theta = 8,\ n = 177$	$p_o = 10,\ p_\theta = 10,\ n = 300$	$p_o = 11,\ p_\theta = 13,\ n = 459$
1	511.440	511.387	511.150	511.112	511.105	511.091	511.083	511.081
2	645.576	645.291	645.193	644.977	644.960	644.897	644.870	644.865
3	903.155	886.217	902.552	886.334	886.310	886.168	885.608	885.593
4	——	——	1313.95	1307.35	1301.27	1236.40	1231.88	1231.77

Table 3 Linear frequencies of CCCC rectangular plates (radians per second) computed by HFEM

	$b/h=1000$		$b/h=100$		$b/h=50$		$b/h=25$		$b/h=10$	
Mode	CPT[a]	FSDT[b]	CPT	FSDT	CPT	FSDT	CPT	FSDT	CPT	FSDT
1	163.643	163.634	1636.43	1626.60	3272.87	3196.40	6545.74	5994.46	16364.3	11118.4
2	206.488	206.475	2064.88	2051.76	4129.75	4028.51	8259.51	7544.86	20648.8	14176.3
3	283.583	283.566	2835.84	2816.53	5671.67	5523.61	11343.3	10317.7	28358.4	19382.6
4	394.472	394.474	3944.72	3914.62	7889.45	7658.41	15778.9	14187.0	39447.2	22822.4

[a] $p_o=10$ and $n=100$. [b] $p_o=10$, $p_\theta=10$, and $n=300$.

Table 4 Nonlinear frequency ratios $\omega/\omega_{\ell 1}$, first mode, $\xi=0$, and $\eta=0$

Thin-plate theory,[3] $p_o=5$ and $p_i=7$		FSDT, $p_o=5$, $p_i=7$, and $p_\theta=7$	
$w_{\max}/h$	$\omega/\omega_{\ell 1}$	$w_{\max}/h$	$\omega/\omega_{\ell 1}$
0.19992	1.0055	0.2000	1.0055
0.61101	1.0508	0.6000	1.0491
0.99977	1.1324	1.0000	1.1326
1.4976	1.2816	1.5000	1.2826

Table 5 Nonlinear frequency ratios $\omega/\omega_{\ell 1}$, second mode, $\xi=0.4$, and $\eta=0$

Thin-plate theory,[3] $p_o=5$ and $p_i=7$		FSDT, $p_o=5$, $p_i=7$, and $p_\theta=7$	
$w_{\max}/h$	$\omega/\omega_{\ell 1}$	$w_{\max}/h$	$\omega/\omega_{\ell 1}$
0.20030	1.2781	0.2000	1.2780
0.60010	1.3981	0.6000	1.3982
0.99745	1.6076	1.0000	1.6094
1.5021	1.9611	1.5000	1.9600

Table 6 Nonlinear frequency ratios $\omega/\omega_{\ell 1}$, third mode, $\xi=0$, and $\eta=0$

Thin-plate theory,[3] $p_o=5$ and $p_i=7$		FSDT, $p_o=5$, $p_i=7$, and $p_\theta=7$	
$w_{\max}/h$	$\omega/\omega_{\ell 1}$	$w_{\max}/h$	$\omega/\omega_{\ell 1}$
0.20094	1.7962	0.2000	1.7956
0.59930	2.2131	0.6000	2.2145
1.0004	2.8936	1.0000	2.8940

theory was followed, are also shown for comparison purposes. In Table 3, plate 2 is again considered, but with different thicknesses: $b/h=1000$, $b/h=100$, $b/h=50$, $b/h=25$, and $b/h=10$.

Tables 2 and 3 demonstrate again the validity of the approach followed. For very thin plates ($b/h=1000$), very good agreement is found between the thin-plate theory values and those from thick-plate theory, showing that the proposed element is not prone to shear locking. This had also been found in p-version elements for isotropic materials.[18,19] As expected, the natural frequencies calculated with the FSDT plate theory are lower than those calculated with the classical thin-plate theory (CPT). The thicker the plate and the higher the mode, the more natural frequencies differ when computed using the different p elements.

Although the FSDT p-version finite element proposed requires a quite moderate number of DOF for convergence, this number is larger than that required by the thin-plate p element because the rotations are not independent in the latter. In fact, after neglecting in-plane inertia and condensing the equations of motion, a thin-plate hierarchical finite element has a total of $n=p_o^2$ DOF, whereas the FSDT plate element has $n=p_o^2+p_{\theta_x}^2+p_{\theta_y}^2$ DOF. Therefore, the FSDT p element is more demanding computationally than the CPT. To give an idea of the difference in computational cost, the CPU time necessary to compute the natural frequencies of the plate $b/h=1000$, Table 3, was determined. If FORTRAN is used, both models, even considering in-plane displacements

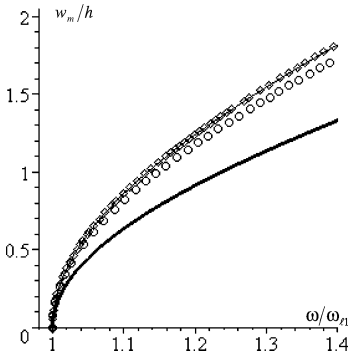

a) First mode, $\xi=\eta=0$

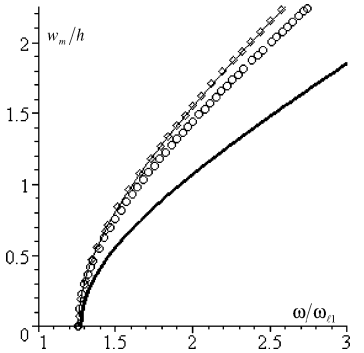

b) Second mode, $\xi=0.4$ and $\eta=0$

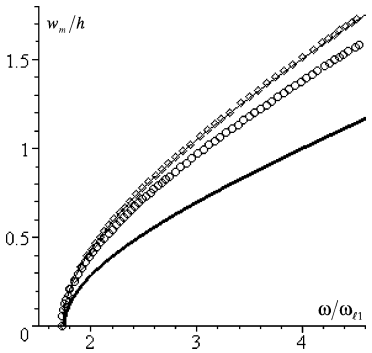

c) Third mode, $\xi=0$ and $\eta=0$

Fig. 2 Backbone curves $a/b=1.5$: ——, $b/h=10$; ○, $b/h=25$; ——, $b/h=100$; and ◇, $b/h=1000$.

($p_i=p_o=p_\theta=10$), provide results rather quickly: The 300 DOF CPT p element requires 1 s or less, whereas the 500 DOE FSDT p element requires around 2 s. (These times are approximated because the code employed only gives CPU time in seconds.) Another term of comparison was obtained using a symbolic manipulator package and reduced models (without in-plane inertia), where the thin-plate element (100 DOF) provided results around 23 times faster than the FSDT plate element (300 DOF).

B. Nonlinear Dynamics

The study carried out in the preceding section showed that the $p_o=5$, $p_i=p_\theta=7$, 123-DOF element is quite accurate for fully

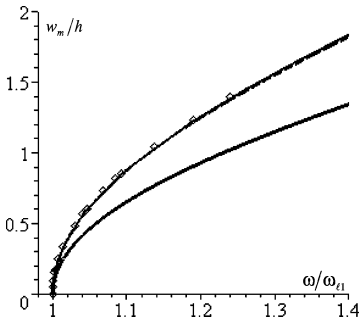

a) First mode, $\xi = \eta = 0$

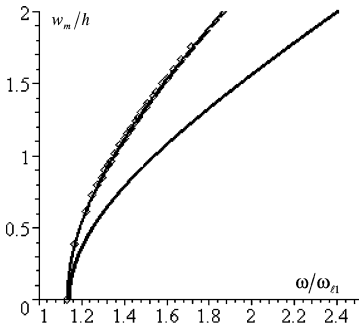

b) Second mode, $\xi = 0.4$ and $\eta = 0$

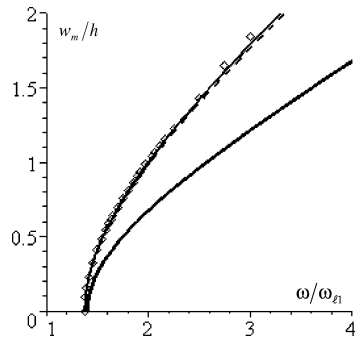

c) Third mode, $\xi = 0$ and $\eta = 0$

Fig. 3 Backbone curves *a/b* = 2.0: ——, *b/h* = 10; – – –, *b/h* = 50; ——, *b/h* = 100; and ◇, *b/h* = 1000.

clamped plates, and this element is now used to analyze the nonlinear vibrations of plates with clamped boundaries. In the next paragraphs, the importance of different parameters in the plates' dynamic behavior is analyzed. These parameters are the thickness of the plates, the aspect ratio, and the orientation of the fibers. The geometrical and material parameters are essentially those of plate 2; in the first set of examples, θ is equal to 45 deg.

Tables 4–6 list the first three nonlinear natural frequencies of vibration of plate 2, with $h = 0.001$ m, as a function of the vibration amplitude. This is a thin plate, and very good agreement is found between the thin-plate theory values published in Ref. 3 and the FSDT results computed and described herein.

Figures 2 and 3 display the backbone curves of rectangular plates with aspect ratios $a/b = 1.5$ and 2.0 ($a = 0.48$ m), and with various thicknesses. Here, w_m is the amplitude of vibration displacement at the coordinates indicated. The hard spring effect changes with the thickness of the plates, and the rate of change depends on the mode analyzed, being the variation of the resonance frequency with the vibration amplitude greater for higher-order modes than for the first one. This probably occurs because, for the same vibration amplitude, higher-order modes imply larger slopes on the deformed plate and, consequently, larger stresses and strains. The behavior of the thinner plates varies slightly with the thickness, but the difference between the $b/h = 100$ and 25 plates is quite significant.

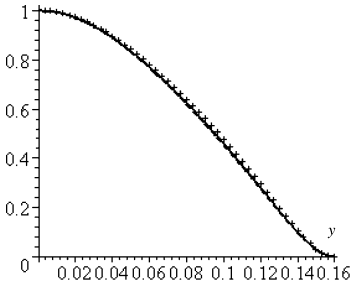

a) *b/h* = 10 and w_m/h: – – –, 0.53; ——, 0.499; and +, 0.998

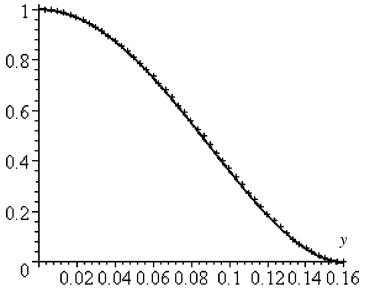

b) *b/h* = 100 and w_m/h: – – –, 0; ——, 0.50; and +, 0.999

Fig. 4 Sections *x* = 0 of normalized first nonlinear mode shapes of rectangular plate *a/b* = 1.5 at different vibration displacement amplitudes, w_m calculated at (0,0).

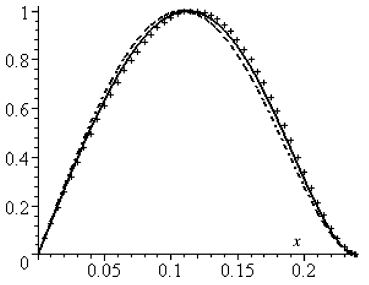

a) *b/h* = 10 and w_m/h: – – –, 0; ——, 500; and +, 1.001

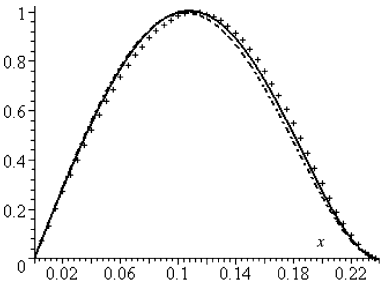

b) *b/h* = 100 and w_m/h: – – –, 0; ——, 0.500; and +, 0.999

Fig. 5 Sections at *x* = 0 of normalized second nonlinear mode shapes of a rectangular plate *a/b* = 1.5 at different vibration displacement amplitudes, w_m calculated at *x* = 0.4 *a*/2 and *y* = 0.

Figures 4–6 show the normalized nonlinear mode shapes of rectangular plates when $a/b = 1.5$ and at different vibration displacement amplitudes. The nondimensional displacement amplitudes w_m/h of the first and third modes are calculated at $\xi = \eta = 0$, and those of the second mode at $\xi = 0.4$ and $\eta = 0$. The curves were normalized to facilitate comparison between them.

As with thin-plate theory,[1–4] the mode shape changes with the amplitude of vibration and the variation is smooth in the case of harmonic motions. For the second and third modes, the point of maximum vibration amplitude approaches the clamped edges as

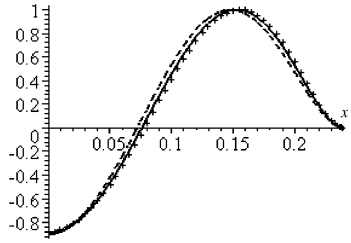

a) $b/h = 10$ and w_m/h: – – –, 0; ——, 498; and +, 1.000

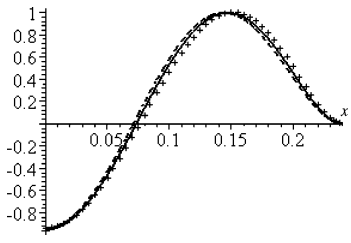

b) $b/h = 100$ and w_m/h: – – –, 0;——, 0.500; and +, 1.000

Fig. 6 Sections $y = 0$ of normalized third nonlinear mode shapes of rectangular plate $a/b = 1.5$ at different vibration displacement amplitudes (w_m calculated at $x = 0$ and $y = 0$).

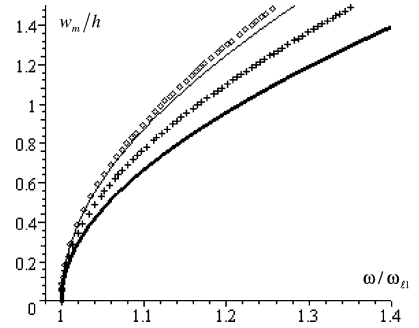

a) First mode $(\xi, \eta) = (0, 0)$

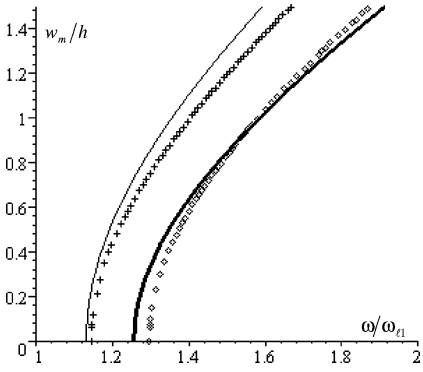

b) Second mode $(\xi, \eta) = (0.4, 0)$

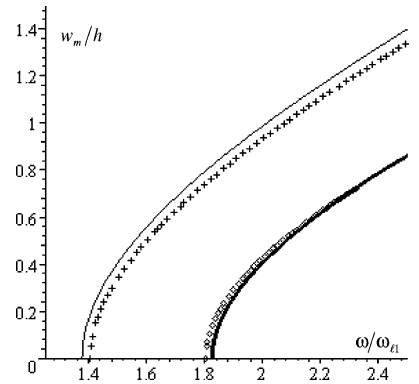

c) Third mode $(\xi, \eta) = (0, 0)$

Fig. 7 Backbone curves: ◇, $\theta = 30$ deg; ——, $\theta = 45$ deg; +, $\theta = 60$ deg; and ——, $\theta = 90$ deg.

the amplitude of vibration increases. A similar effect was reported in Ref. 29 concerning the second nonlinear mode of isotropic thin plates. The alteration in the mode shape is slightly larger for thicker than for thin plates.

This section is concluded with the investigation of the effect of the fiber orientation, θ. Plate 2, with $b = a/2$ and $h = b/50$ is used as an example, and the values considered for θ are 30, 45, 60, and 90 deg. The fundamental linear frequencies are, respectively, 3306.95, 4095.08, 3774.48, and 3351.50 rad/s.

Figure 7 displays the backbone curves of the first three modes of vibration for different fiber orientations. In the first mode of vibration, it is evident that the hardening spring effect increases as θ increases. Consequently, the nonlinear fundamental frequency at vibration amplitudes equal to h is 3691.1 rad/s for the $\theta = 30$ deg plate and 4079.2 rad/s for the $\theta = 90$ deg plate. That is, whereas the linear frequencies of these two plates only differ by 1.3%, the nonlinear frequencies at a vibration amplitude equal to the plates thicknesses differ by 10.5%. The hardening spring effect of higher-order modes also varies with the fiber orientations.

Recall that a linear elastic relation between stress and strain was assumed. The consideration of plasticity and failure, due to delamination or another cause, is not in the objective of this work, but will be necessary for greater accuracy and for real life applications. This becomes particularly true in the case of large-amplitude vibrations of the rather thick plate $b/h = 10$, which is used here as a limiting case.

IV. Conclusions

A first-order shear deformation, laminated composite plate, p-version HFEM was presented. When the convergence properties were studied and results compared with published results, it was demonstrated that the element proposed requires a moderate number of DOF for accuracy. Moreover, it can be applied to study thick and thin plates because no shear locking effects were found. However, because independent rotation fields are necessary, it requires more DOF than its thin-plate element counterpart.

For thick plates with different aspect ratios, it was found that the first and higher nonlinear mode shapes of vibration vary with the amplitude of displacement achieved. It was also verified in the numerical experiments that the hardening spring effect is more accentuated for thicker than for thin plates and that it tends to increase with the order of the mode under analysis.

A parameter that can be easily varied to obtain different properties is the angle of orientation of the fibers. As an example, it was verified for a $(2\theta, -\theta, \theta\ 0)_{\text{sym}}$ plate that the hardening spring effect of the first mode increases as θ increases from 30 to 90 deg.

In summary, both in linear and in nonlinear vibration, the difference between the thick- and the thin-plate element results can be quite large for thicker plates and for higher-order modes, where the application of the p-version hierarchical finite thick-plate element is fully justified. For low-order modes of thin plates, the p-version element based on CPT is advised because the smaller number of DOF results in a much lower computational cost.

The analysis carried out here regards only the mode shapes and natural frequencies and will be valid as long as the nonlinear free vibrations are approximately harmonic. The p-version thick-plate element will have additional advantages in the computation of stresses and in the analysis of nonharmonic oscillations, in the latter case because higher-order modes may couple with the lower-order modes.

Appendix: Strain-Displacement Relations

By the use of relation (12) and the same shape functions for the displacements u and v, the following strain-displacement relations are defined:

$$\left\{\varepsilon_0^p\right\} = \begin{bmatrix} \left\{N^u_{,x}\right\}^T & 0 \\ 0 & \left\{N^u_{,y}\right\}^T \\ \left\{N^u_{,y}\right\}^T & \left\{N^u_{,x}\right\}^T \end{bmatrix} \begin{Bmatrix} q_u \\ q_v \end{Bmatrix} \tag{A1}$$

$$\left\{\varepsilon_o^b\right\} = \begin{bmatrix} -\left\{N_{,x}^{\theta_y}\right\}^T & 0 \\ 0 & \left\{N_{,y}^{\theta_x}\right\}^T \\ -\left\{N_{,y}^{\theta_y}\right\}^T & \left\{N_{,x}^{\theta_x}\right\}^T \end{bmatrix} \begin{Bmatrix} q_{\theta_y} \\ q_{\theta_x} \end{Bmatrix} \tag{A2}$$

$$\left\{\varepsilon_L^p\right\} = \begin{Bmatrix} \frac{1}{2}\{q_w\}^T \left\{N_{,x}^w\right\}\left\{N_{,x}^w\right\}^T\{q_w\} \\ \frac{1}{2}\{q_w\}^T \left\{N_{,y}^w\right\}\left\{N_{,y}^w\right\}^T\{q_w\} \\ \{q_w\}^T \left\{N_{,x}^w\right\}\left\{N_{,y}^w\right\}^T\{q_w\} \end{Bmatrix} \tag{A3}$$

$$\begin{Bmatrix} \gamma_{zx} \\ \gamma_{yz} \end{Bmatrix} = \begin{bmatrix} \left\{N_{,x}^w\right\}^T & \{N^{\theta_y}\}^T & 0 \\ \left\{N_{,y}^w\right\}^T & 0 & -\{N^{\theta_x}\}^T \end{bmatrix} \begin{Bmatrix} q_w \\ q_{\theta_y} \\ q_{\theta_x} \end{Bmatrix} \tag{A4}$$

Acknowledgments

The support of this work by the Portuguese Science and Technology Foundation and Fundo Europeu de Desenvolvimento Regional (FEDER), under Project POCTI/1999/EME/32641, is gratefully acknowledged.

References

[1]Han, W., and Petyt, M., "Geometrically Nonlinear Vibration Analysis of Thin, Rectangular Plates Using the Hierarchical Finite Element Method—I: The Fundamental Mode of Isotropic Plates," *Computers and Structures*, Vol. 63, No. 2, 1997, pp. 295–308.

[2]Han, W., and Petyt, M., "Geometrically Nonlinear Vibration Analysis of Thin, Rectangular Plates Using the Hierarchical Finite Element Method—II: 1st Mode of Laminated Plates and Higher Modes of Isotropic and Laminated Plates," *Computers and Structures*, Vol. 63, No. 2, 1997, pp. 309–318.

[3]Ribeiro, P., and Petyt, M., "Nonlinear Vibration of Composite Laminated Plates by the Hierarchical Finite Element and Continuation Methods," *Composite Structures*, Vol. 46, No. 3, 1999, pp. 197–208.

[4]Ribeiro, P., and Petyt, M., "Multi-modal Geometrical Non-linear Free Vibration of Fully Clamped Composite Laminated Plates," *Journal of Sound and Vibration*, Vol. 225, No. 1, 1999, pp. 127–152.

[5]Mei, C., and Decha-Umphai, K., "Finite Element Method for Nonlinear Forced Vibrations of Rectangular Plates," *AIAA Journal*, Vol. 23, No. 7, 1985, pp. 1104–1110.

[6]Zienkiewicz, O. C., and Taylor, R. L., *The Finite Element Method*, 4th ed., McGraw–Hill, London, 1988.

[7]Sathyamoorthy, M., "Nonlinear Vibration Analysis of Plates: A Review and Survey of Current Developments," *Applied Mechanics Review*, Vol. 40, No. 11, 1987, pp. 1553–1561.

[8]Reissner, E., "The Effect of Transverse Shear Deformation on the Bending of Elastic Plates," *Journal of Applied Mechanics*, Vol. 12, No. 2, 1945, pp. 69–77.

[9]Mindlin, R. D., "Influence of Rotatory Inertia and Shear on Flexural Vibrations of Isotropic, Elastic Plates," *Journal of Applied Mechanics*, Vol. 18, No. 1, 1951, pp. 31–38.

[10]Petyt, M., *Introduction to Finite Element Vibration Analysis*, Cambridge Univ. Press, Cambridge, England, U.K., 1990, p. 35 and Chap. 6.

[11]Mei, C., and Prasad, C. B., "Effects of Large Deflection and Transverse Shear on Response of Rectangular Symmetric Composite Laminates Subjected to Acoustic Excitation," *Journal of Composite Materials*, Vol. 23, No. 6, 1989, pp. 606–639.

[12]Reddy, J. N., and Chao, W. C., "Large Deflection and Large-Amplitude Free Vibrations of Laminated Composite-Material Plates," *Computers and Structures*, Vol. 13, Nos. 1–3, 1981, pp. 341–347.

[13]Hinton, E., and Owen, D. R. J., *Finite Element Software for Plates and Shells*, Pineridge Press, 1984, Chap. 3.

[14]Tessler, A., and Hughes, T. J. R., "A Three-Node Mindlin Plate Element with Improved Transverse Shear," *Computer Methods in Applied Mechanics and Engineering*, Vol. 50, No. 1, 1985, pp. 71–101.

[15]Chen, W. C., and Liu, W. H., "Deflections and Free Vibrations of Laminated Plates—Levy Type Solutions," *International Journal of Mechanical Sciences*, Vol. 32, No. 9, 1990, pp. 779–793.

[16]Ganapathi, M., Varadan, T. K., and Sarma, S. M., "Nonlinear Flexural Vibrations of Laminated Orthotropic Plates," *Computers and Structures*, Vol. 39, No. 6, 1991, pp. 685–688.

[17]Soldatos, K. P., and Messina, A., "The Influence of Boundary Conditions and Transverse Shear on the Vibration of Angle-Ply Laminated Plates, Circular Cylinders and Cylindrical Panels," *Computer Methods in Applied Mechanics and Engineering*, Vol. 190, No. 18–19, 2001, pp. 2385–2409.

[18]Rank, E., Holzer, S., and Werner, H., "An Implementation of the $h-p$ Version of the Finite Element Method for the Reissner–Mindlin Plate Problems," *International Journal for Numerical Methods in Engineering*, Vol. 30, No. 3, 1990, pp. 459–471.

[19]Scapolla, T., "Avoiding Locking in Reissner–Mindlin Plates with High-Order Hierarchic Bubble Plus Finite Elements," *Journal of Computational and Applied Mathematics*, Vol. 63, No. 1–3, 1995, pp. 291–299.

[20]Brockman, R. A., "Dynamics of the Bilinear Mindlin Plate Element," *International Journal for Numerical Methods in Engineering*, Vol. 24, No. 12, 1987, pp. 2343–2356.

[21]Qian, G.-L., Hoa, S. V., and Xiao, X., "A New Rectangular Plate Element for Vibration Analysis of Laminated Composites," *Journal of Vibration and Acoustics*, Vol. 120, No. 1, 1998, pp. 80–86.

[22]Reddy, J. N., "Theory and Analysis of Laminated Composite Plates," *Mechanics of Composite Materials and Structures*, edited by C. A. M. Soares, C. A. M. Soares, and M. J. M. Freitas, Kluwer Academic, Dordretch, The Netherlands, 1999, pp. 1–62.

[23]Szabó, B. A., and Mehta, A. K., "p-Convergent Finite Element Approximations in Fracture Mechanics," *International Journal for Numerical Methods in Engineering*, Vol. 12, No. 3, 1978, pp. 551–560.

[24]Szabó, B. A., and Babuska, I., *Finite Element Analysis*, Wiley, New York, 1991.

[25]Bardell, N. S., "Free Vibration Analysis of a Flat Plate Using the Hierarchical Finite Element Method," *Journal of Sound and Vibration*, Vol. 151, No. 2, 1991, pp. 263–289.

[26]Vinson, J. R., and Sierakowski, R. L., *The Behavior of Structures Composed of Composite Materials*, Martinus Nijhoff, Dordrecht, The Netherlands, 1987, pp. 43–47.

[27]Noor, A. K., and Burton, W. S., "Stress and Free Vibration Analyses of Multilayered Composite Plates," *Composite Structures*, Vol. 11, No. 3, 1989, pp. 183–204.

[28]Sivakumaran, K. S., "Frequency Analysis of Symmetrically Laminated Plates with Free Edges," *Journal of Sound and Vibration*, Vol. 125, No. 2, 1988, pp. 211–225.

[29]El Kadiri, M., Benamar, R., and White, R. G., "The Non-linear Free Vibration of Fully Clamped Rectangular Plates: Second Non-linear Mode for Various Plate Aspect Ratios," *Journal of Sound and Vibration*, Vol. 228, No. 2, 1999, pp. 333–358.

S. Saigal
Associate Editor